Heat Flux Estimates for the Western North Atlantic. Part I: Assimilation of Satellite Data into a Mixed Layer Model*

KATHRYN A. KELLY

Department of Physical Oceanography, Woods Hole Oceanographic Institution, Woods Hole, Massachusetts

BO QIU

Department of Oceanography, University of Hawaii at Manoa, Honolulu, Hawaii

(Manuscript received 26 April 1994, in final form 9 March 1995)

ABSTRACT

Satellite-derived temperature and geostrophic velocities were assimilated into a mixed layer model to obtain estimates of the net surface heat flux as the residual of the upper ocean heat budget. The heat budget included eddy diffusion, advection, and vertical entrainment. Assimilation was done using a Kalman filter on both the temperature tendency and the temperature of the mixed layer. The error in temperature tendency was used to derive a new surface heat flux estimate. Experiments performed on the actual data suggested that better surface flux estimates could be obtained by allowing the model to predict the mixed layer depth than by adjusting the depth to a climatological value. A systematic error in the temperature tendency appeared to be due to errors in the estimate of the mean sea surface height from the altimeter; a partial correction for these errors was computed. The agreement between the time series of spatially averaged surface flux and that obtained from the ECMWF atmospheric model was surprisingly good. The temporally averaged surface flux estimates from the mixed layer model were in good agreement with the Bunker climatological values, except in February and March, when the model mixed layer shoaled more rapidly than expected from climatology.

1. Introduction

Although the largest values of the net surface heat flux in the North Atlantic occur in the western North Atlantic (Isemer and Hasse 1987), this region is the most difficult one in which to attempt a heat budget because of the strong currents and large temperature gradients. In previous efforts to balance the upper ocean heat budget (for example, Stevenson and Niiler 1983; Paduan et al. 1988) regions of strong currents were avoided because a heat budget near a western boundary current, with speeds as large as 2 m s^{-1}, requires an accurate estimate of the contribution of advection. In the tropical Pacific surface heat fluxes estimated from satellite data using bulk parameterizations have been shown to account for a significant fraction of the observed variance in SST (Liu and Gautier 1990); however, the strong currents and eddies in a boundary current region may significantly alter the balance that determines the SST because both advection and eddy surface fluxes are important. Now, however, the availability of surface velocity fields from the radar altimeter, along with the high spatial resolution temperature fields from infrared sensors, suggests that estimates of the heat budget in western boundary currents are feasible.

An analysis of the heat budget for the North Pacific was performed by Qiu and Kelly (1993, hereafter QK) using a numerical model of the upper ocean mixed layer, combined with heat flux estimates from the European Centre for Medium-Range Weather Forecasts (ECMWF) and velocities from the Geosat altimeter. The simple mixed layer model included vertical entrainment of the cold water beneath the mixed layer and heating by the surface flux, as well as diffusion and advection. The importance of advection in the North Pacific for the seasonal heat budget was shown in this analysis: cooling by advection offset nearly 30% of the surface warming due to the atmosphere (QK).

The method for obtaining the heat budget estimate in the North Atlantic differs from that for the North Pacific in that the mixed layer model is essentially run in an inverse mode to obtain estimates of the net surface heat flux. In the North Pacific, we specified surface flux and obtained a prediction for mixed layer

* Woods Hole Oceanographic Institution Contribution Number 8716.

Corresponding author address: Dr. Kathryn A. Kelly, Department of Physical Oceanography, Woods Hole Oceanographic Institution, Woods Hole, MA 02543.
E-mail: kkelly@whoi.edu

temperature; here, we require that the model match the temporal change in temperature, or temperature tendency, specified from AVHRR data, and estimate the surface flux required to match the temperature tendency. The matching between observed and modeled temperature tendency is done using a Kalman filter. The relationship between surface flux and temperature tendency depends critically upon mixed layer depth, which is predicted by the model. The net surface heat flux is usually estimated using bulk parameterizations, which are functions of air temperature, humidity, cloud cover, wind stress, and sea surface temperature (SST). These parameterizations are particularly difficult to make in western boundary current regions, where horizontal scales of the variables are a few tens of kilometers, an order of magnitude smaller than those in the open ocean. The method described here is nearly the reverse formulation of a method developed by Yan et al. (1990), in which the mixed layer depth is inferred from changes in SST, using simple parameterizations for heat fluxes in terms of SST and wind speed.

Besides producing estimates of net surface heat flux, we wished to examine the effect of seasonal-to-interannual fluctuations in the Gulf Stream (GS) intensity on the mixed layer heat budget. During the Exact Repeat Mission of the Geosat altimeter (November 1986–April 1989), the GS jet position and surface transport (the height difference across the jet) fluctuated with a dominant period of about 9 months and with a trend toward smaller surface transports (Kelly and Watts 1994). Similar fluctuations in jet intensity and position were observed in the Kuroshio Extension (Qiu et al. 1991), with a trend toward larger surface transports.

Part I contains the description of the method used to estimate the surface flux, beginning with a description of the numerical model in section 2, which is the same as that used by QK. Section 3 gives the essential formulation of the Kalman filter and the specific modifications for this application. Section 4 briefly describes the processing of the several fields of variables used in this study. The testing of the model on synthetic data and the implications for studies on the real data is discussed in section 5. The application of the Kalman filter to the real data and a discussion of the results are contained in sections 6 and 7, respectively, which are followed by a summary and conclusions. An analysis of the heat budget is contained in Part II.

2. Formulation of the numerical model

The numerical model for the upper ocean mixed layer is described in detail in QK and a brief description is included here for the reader's convenience, with an emphasis on the changes needed to assimilate the satellite data. The upper ocean heat budget is given in terms of changes in the mixed layer temperature T_m and depth h_m as follows:

$$\frac{\partial h_m}{\partial t} + \frac{\partial U}{\partial x} + \frac{\partial V}{\partial y} = A_h \nabla^2 h_m + w_e \tag{1}$$

$$h_m \frac{\partial T_m}{\partial t} + U \frac{\partial T_m}{\partial x} + V \frac{\partial T_m}{\partial y} = h_m A_T \nabla^2 T_m + \frac{Q_{\text{net}} - q(-h_m)}{c_p \rho_0} - \Delta T w_e, \tag{2}$$

where

$$V = -f^{-1}\left(-g h_m \frac{\partial \eta}{\partial x} + \frac{\alpha g h_m^2}{2} \frac{\partial T_m}{\partial x} + \frac{\tau^x}{\rho_0} \right) \tag{3}$$

$$U = f^{-1}\left(-g h_m \frac{\partial \eta}{\partial y} + \frac{\alpha g h_m^2}{2} \frac{\partial T_m}{\partial y} + \frac{\tau^y}{\rho_0} \right) \tag{4}$$

are the horizontal transports in the mixed layer, (τ^x, τ^y) the wind stress, c_p the specific heat of water, ρ_0 the reference density, A_T (A_h) is subgrid-scale horizontal eddy diffusivity for temperature (mixed layer depth), and Q_{net} the net heat flux through the ocean surface. The downward radiative heat flux at the bottom of the mixed layer, $q(-h_m)$, is included to account for possible penetration through the shallow mixed layer in summer. The temperature difference between the mixed layer and the water below, ΔT, was taken as fixed. The velocity term is the sum of the geostrophic and the Ekman components for transport, which includes a shear term based on the mixed layer temperature gradients. To close these equations requires a parameterization of the entrainment velocity w_e. Based on model tests using realistic surface fluxes and climatological SST we chose a relatively precise formulation of the turbulent kinetic energy balance, as in QK. The numerical model covers the area from 33° to 43°N and from 75° to 55°W (Fig. 1), with grid spacing of 0.5° in latitude and 1° in longitude. These scales were determined primarily by the resolution of the altimeter observations.

Advection and diffusion were computed only for interior grid points for both mixed layer temperature T_m and depth h_m. For temperature, boundary values were computed using (2) without the advection and diffusion terms, except along the eastern boundary, where $\partial T_m/\partial x = 0$. Along all boundaries the gradient of h_m normal to the boundary was set to zero; that is, $\partial h_m/\partial n = 0$.

We performed test runs in which the mixed layer temperature and depth using the ECMWF wind and surface flux data were prognostically predicted for a two-year period (Fig. 2). These tests allowed us to tune the model parameter ΔT in (2); a fixed value of 0.5°C allowed the numerical model to adequately simulate the seasonal cycle of both h_m and T_m. The values shown in Fig. 2 are similar to those computed from

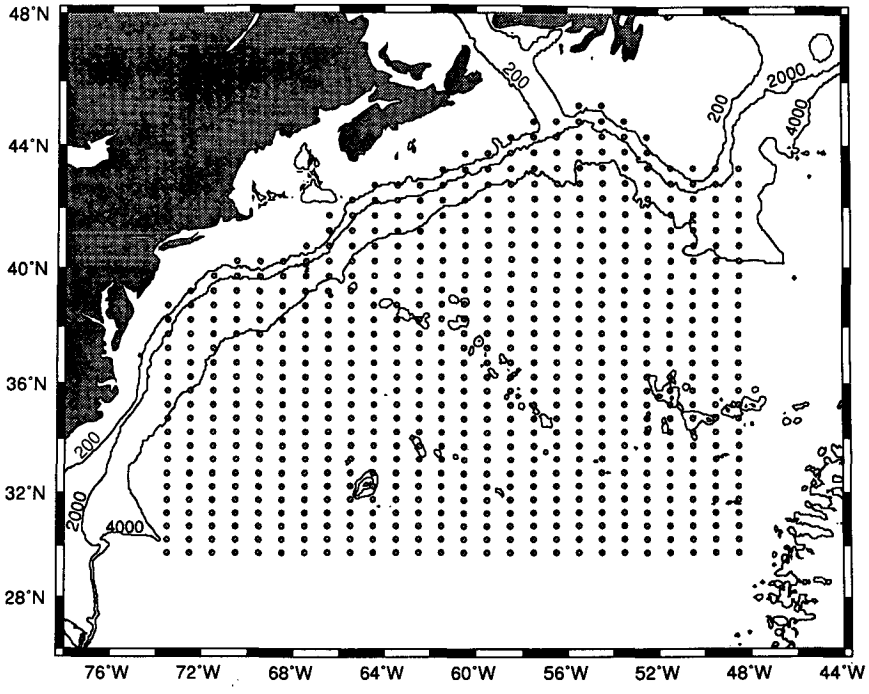

FIG. 1. Domain of the numerical mixed layer model. The model resolution was 0.5° latitude and 1° longitude with the northern boundary along the 2000-m isobath. Also shown are the 200-m, 2000-m and 4000-m isobaths.

the Levitus climatology (1982), as shown in Part II (Figs. 11a,12).

For the data assimilations, the model was run for one week at a time using a time step of two hours and prescribed winds. At the end of each week, a new surface flux estimate was made and the mixed layer temperature T_m and the mixed layer depth h_m were adjusted using the temperature data. The initial mixed layer temperature for the first week was derived from the AVHRR data, and the initial surface flux estimate for the first week only was taken from the ECMWF data.

3. Data assimilation using a simple Kalman filter

An approximate version of a Kalman filter was used to assimilate the data and to make the surface flux estimates. The advantage of using a Kalman filter is the ability to incorporate error estimates into the adjustment of the variables; however, the disadvantage is the prohibitive computational requirements. To reduce the computational burden, one can either simplify the physics of the problem and use the exact Kalman filter formulation, or one can use the full physics and an approximate form of the Kalman filter (see, for example, Fukumori et al. 1993). We chose the latter option because we wanted to accurately represent the effects of advection and diffusion, which require the highest possible spatial resolution consistent with the available data.

a. Basic Kalman filter

The Kalman (1960) filter formulation requires that the problem be posed as a set of linear operations on the "state vector" $\mathbf{q}$, which contains those variables which will be predicted and for which observations are available. For example, using the notation of Gaspar and Wunsch (1989), the new state vector $\mathbf{q}(k|k-1)$ at time k is predicted from the state vector at time $k-1$ using the state transition matrix $\mathbf{A}$ as

$$\mathbf{q}(k|k-1) = \mathbf{A}(k-1)\mathbf{q}(k-1|k-1) + w(k-1), \quad (5)$$

where $w(k-1)$ is that part of the physics that does not involve the state variables. The notation $(k|k-1)$ indicates that only information available at the previous time step was used to make this estimate, as opposed to the notation $(k|k)$, which suggests that additional information (i.e., data from time k) was used in the prediction. For example, if the state variables were the mixed layer temperatures at each model grid point, then (2) could be rewritten to predict the temperature at time k, given the temperature at time $k-1$, as

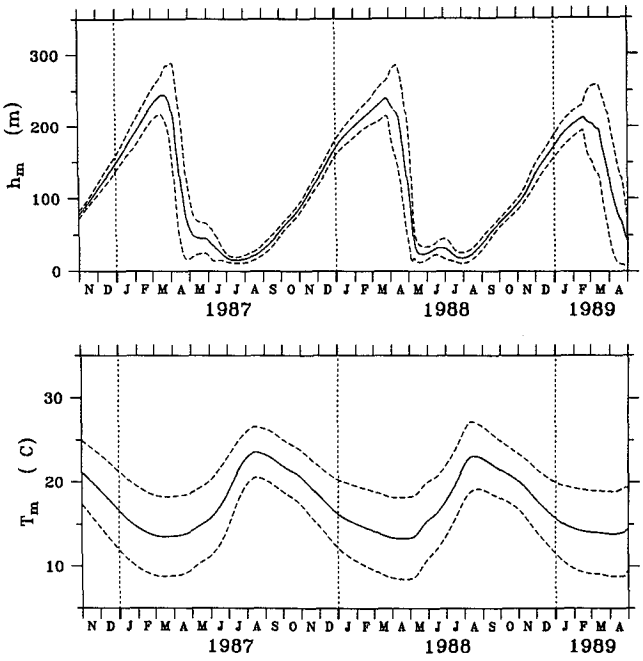

FIG. 2. Annual cycle of (a) mixed layer depth and (b) temperature from the numerical mixed layer model. The model was run with specified surface heat flux and wind forcing to determine its accuracy in producing the annual cycle. Solid lines are the monthly mean depth and temperature and dashed lines are an estimate of the standard deviation for each month.

$$T_m(k|k-1) = T_m(k-1) - \delta t \frac{U}{h_m}\frac{\partial T_m(k-1)}{\partial x} - \delta t \frac{V}{h_m}\frac{\partial T_m(k-1)}{\partial y} + \delta t A_h \nabla^2 T_m(k-1) + \delta t\left[\frac{Q_{\text{net}} - q(-h_m)}{c_p \rho_0 h_m}\right] - \delta t w_e[\Delta T/h_m], \quad (6)$$

where δt is the time step and $T_m(k-1|k-1)$ is implied. Expanding the spatial derivatives of $T_m(k-1)$ in finite differences gives a set of linear equations to predict $T_m(k|k-1)$; all coefficients of T_m would be contained in $\mathbf{A}$ and the remaining terms would constitute w.

The error associated with this estimate of q can be written as

$$\mathbf{P}(k|k-1) = \mathbf{A}(k-1)\mathbf{P}(k-1|k-1) \times \mathbf{A}^{\mathrm{T}}(k-1) + \boldsymbol{\Gamma}(k-1), \quad (7)$$

where $\mathbf{P}(k|k-1)$ is the covariance matrix of the error propagated from time $k-1$ by the state transition matrix. For example, temperature errors resulting from errors in the specified surface flux Q_{net} are advected to nearby grid points. In addition to the propagated error, the model makes a new error at each time step due to imperfect physics, which is denoted by the covariance matrix $\boldsymbol{\Gamma}$.

Both $\mathbf{q}(k|k-1)$ and $\mathbf{P}(k|k-1)$ constitute predictions that can be refined when observations and error estimates for those observations are available. Using observations available at time k, a revised estimate of $\mathbf{q}$ can be computed as an error-weighted average of the model prediction $\mathbf{q}(k|k-1)$ and the data $\mathbf{d}$, as

$$\mathbf{q}(k|k) = \mathbf{q}(k|k-1) + \mathbf{G}(k)[\mathbf{d}(k) - \mathbf{q}(k|k-1)]. \quad (8)$$

A similar equation can be written for the revised error estimate as

$$\mathbf{P}(k|k) = [\mathbf{I} - \mathbf{G}(k)]\mathbf{P}(k|k-1), \quad (9)$$

where $\mathbf{I}$ is the identity matrix and $\mathbf{G}$ is the Kalman "gain matrix," which determines the relative importance of the model prediction and the observations. The gain matrix is given by

$$\mathbf{G}(k) = \mathbf{P}(k|k-1)[\mathbf{P}(k|k-1) + \mathbf{R}(k)]^{-1}, \quad (10)$$

where $\mathbf{R}$ is the error covariance matrix for the data d. Relatively large model errors and small data errors will result in a large gain; that is, the prediction will be adjusted to match the data more closely and, conversely, only a small adjustment will be made if data errors are relatively large.

b. *Application of the Kalman filter*

The sequence of steps in the application of the Kalman filter is shown in Fig. 3. The mixed layer model was run for a week and then the quantity Q/h_m was estimated and adjusted toward the temperature ten-

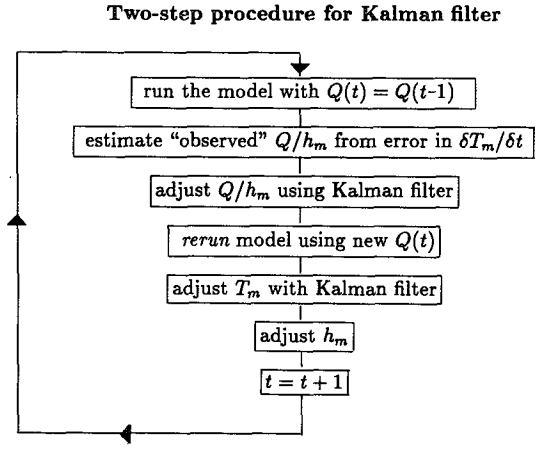

FIG. 3. Flowchart of the two-step Kalman filter. The first application of the Kalman filter adjusted the surface heat flux estimate. The model was then rerun for the same week with the revised estimate, and then the temperature was adjusted.

dency from the data, where we have defined $Q = Q_{net}/(c_p\rho_0)$ for simplicity. The mixed layer model was then rerun for the same week using the new estimate of Q, and then the mixed layer temperature was adjusted toward the temperature data. Thus, the state vector $\mathbf{q}$ for the first step contained Q/h_m, and the state vector for the second step contained mixed layer temperature T_m. The accuracy of the advection and diffusion terms in (2) depends on retaining the sharp gradients of velocity and temperature; therefore, the initial prediction (5) for the state vectors was done using the numerical mixed layer model on a regular grid as in QK. The model was run for a week at a time using a time step of two hours and the final temperature T_m and weekly averaged mixed layer depth h_m were saved. Updates of the state vector (8) and the error covariance (9) using the SST data were performed weekly.

The net surface heat flux was the quantity we wished to estimate, but it is not readily observable. Therefore, the Kalman filter was used to estimate Q/h_m instead. The state transition matrix $\mathbf{A}$ for the first step was the identity matrix; that is, we used the estimate from the previous week as the best guess for the current week:

$$\frac{Q}{h_m}(k|k-1) = \frac{Q}{h_m}(k-1|k-1). \quad (11)$$

The Kalman filter then requires an "observation" of Q/h_m, which we obtained from a linearization of the relationship between temperature tendency and surface flux forcing (2), about the initial estimate; that is,

$$\frac{Q}{h_m}(k|k) = \left[\frac{Q}{h_m}(k|k-1) + \frac{\delta T_d}{\delta t} - \frac{\delta T_m}{\delta t}\right]. \quad (12)$$

Here $\delta T_d/\delta t$ is the finite difference between the weekly optimal maps of SST data at times k and $k-1$, and $\delta T_m/\delta t$ is the finite difference between the weekly model estimates of temperature. By this linearization we have assumed that errors in temperature tendency are due primarily to errors in the estimate of Q/h_m. Although mixed layer depth is a function of Q, a nonlinear correction was found to be small (less than 1%) and was neglected here.

The quantity Q/h_m was expanded in modes, and the coefficients of the modes then became the state variables $\mathbf{q}$. In addition to reducing the computational requirements, the modal decomposition also extracted a relatively smooth surface flux estimate from the imperfectly modeled temperature tendency and the inadequately resolved mesoscale variations in advection. The modes used for temperature tendency were derived from an empirical orthogonal function (EOF) decomposition of the finite differences of weekly SST maps. The modes were computed by factoring the data $dT(t)/dt = \mathbf{USV}^T$, as in Kelly (1988), where $\mathbf{U}$ contains the orthogonal spatial modes and $\mathbf{V}$ contains the time-varying modal amplitudes. The scaling factors in the diagonal matrix $\mathbf{S}$ were retained as part of the modes, so that the modes were given by $\mathbf{F} = \mathbf{US}$. Thus, the coefficients of the modes in the state vectors would be expected to have comparable amplitudes, and additional row scaling of the state transition matrices was not necessary.

After the mixed layer model was rerun using the revised estimate of Q, the temperature was adjusted (Fig. 3). The Kalman adjustment of temperature was also done using a modal decomposition of the temperature anomaly, for computational convenience, rather than to smooth the estimates. In some experiments mixed layer depth was also adjusted in the second step toward climatological values. For these experiments, we used the simple form

$$h_m(k) = h_m + c(h_m^c - h_m), \quad (13)$$

where h_m^c is the climatological mixed layer depth. A formal estimate of the errors as in (7) was not done in these cases because information about the errors was not adequate.

c. *The Kalman smoother*

After the Kalman filter was run on the entire 2.5 years of data, a Kalman smoother of the type used by Gaspar and Wunsch (1989) was used on the amplitudes α of Q/h_m. The smoother essentially runs the Kalman filter in reverse, using the error estimates to generate a smoothed set of amplitudes. This type of smoother does not depend on the original data. The smoothed state vector $\mathbf{q}_{sm}(k)$ and error covariance matrix $\mathbf{P}_{sm}(k)$ are given in terms of the original state vector $\mathbf{q}(k)$ and error covariance matrix $\mathbf{P}(k)$ as

$$\mathbf{q}_{sm}(k) = \mathbf{q}(k|k) + \mathbf{G}_{sm}(k)[\mathbf{q}_{sm}(k+1) - \mathbf{q}(k+1|k)] \quad (14)$$

and

$$\mathbf{P}_{sm}(k) = \mathbf{P}(k|k) + \mathbf{G}_{sm}(k)[\mathbf{P}_{sm}(k+1) - \mathbf{P}(k+1|k)], \quad (15)$$

respectively. The smoother gain matrix is given by

$$\mathbf{G}_{sm}(k) = \mathbf{P}(k|k)\mathbf{A}^T\mathbf{P}^{-1}(k+1|k). \quad (16)$$

Note that the amount of smoothing depends on the error estimates and the original Kalman gain.

4. Maps of variables

The analysis of the upper ocean heat budget required maps of the surface height field η, the surface wind field (τ^x, τ^y), the mixed layer temperature field T_m, and the solar radiation field $q(0)$.

The sea surface height (SSH) data were derived from the Geosat altimeter, which had a repeat cycle of 17 days, using the new orbits and water vapor corrections (Cheney et al. 1991). To eliminate the geoid, which dominates the altimetric height profiles, we com-

puted and subtracted the mean altimetric sea surface from collinear profiles. Subtracting the temporal mean sea surface also removes the temporal mean topography due to ocean currents. Mean sea surface topography profiles relative to the geoid were then synthesized using the method of Kelly and Gille (1990), as modified by Qiu et al. (1991), and added back to the residual heights to obtain total SSH profiles. In this method the Gulf Stream is modeled using a Gaussian velocity profile; the large SSH anomalies created by a narrow jet meandering far from its mean position are exploited to estimate the center position and magnitude of the Gaussian. The single jet model was revised to include recirculation as in Qiu (1992). Details of the computation of the mean SSH are contained in Qiu (1994), along with a comparison of the synthesized mean with the mean dynamic height from climatological data. The absolute surface height data were objectively mapped to the model grid with a 1-day time interval.

The surface wind data used to force the model are the twice-daily 1000-mb wind vectors from ECMWF, with horizontal resolution of 2.5° × 2.5°. Wind vectors were first converted to surface wind stress using the bulk aerodynamic formulae proposed by Trenberth et al. (1990). To ensure that the geostrophic transport and the Ekman transport in (3) and (4) have similar temporal scales, we low-pass filtered the wind stress data and subsampled them daily, as in QK, to eliminate fluctuations shorter than about two weeks. The low-pass filtered data were then linearly interpolated to the model grid.

To estimate the mixed layer temperatures, we used AVHRR data and the optimal average method of Chelton and Schlax (1991), which is an extension of the usual optimal estimate to temporal averages of the data. An optimal average is ideal because it provides error estimates that are needed for the Kalman filter. The AVHRR data were weekly averages, which were initially processed by NOAA using the MCSST algorithm and then interpolated to an 18 km by 18 km grid, by O. Brown at RSMAS. It is necessary to temporally average the SST data first because the data are gappy and, second, because there are relatively large errors in the data, which are uncorrelated from image to image. Appendix A contains a more detailed description of the treatment of the SST data to obtain weekly maps with a nominal two-week averaging interval. Periods of extensive cloud cover (December 1987–January 1988) gave errors nearly a factor of 2 larger than errors for times with clear skies (September 1988 and March 1989; Fig. 4).

Empirical orthogonal functions (EOFs) of both the temperature and the temperature tendency (Fig. 5) were computed from the weekly maps and the finite differences of the weekly maps of the AVHRR data, respectively. Approximately 10% of the maps were excluded from the EOF analyses because the expected errors were large. The temperature modes were dominated by the first mode because the annual signal was not removed; the fraction of variance in the first four modes was 96%, 1%, 0.5%, and 0.4%, respectively. The temperature tendency modes were also dominated by a single mode, although less of the variance was contained in this mode; the fraction of variance in the first four modes was 50%, 4%, 3%, and 2%, respectively. The modes were then smoothed to remove spatial variations smaller than about 3° longitude by 1.5° latitude. The temperature tendency modes were used to estimate the quantity Q/h_m in the first application of the Kalman filter. The temperature modes were used to adjust the temperature in the second application of the Kalman filter.

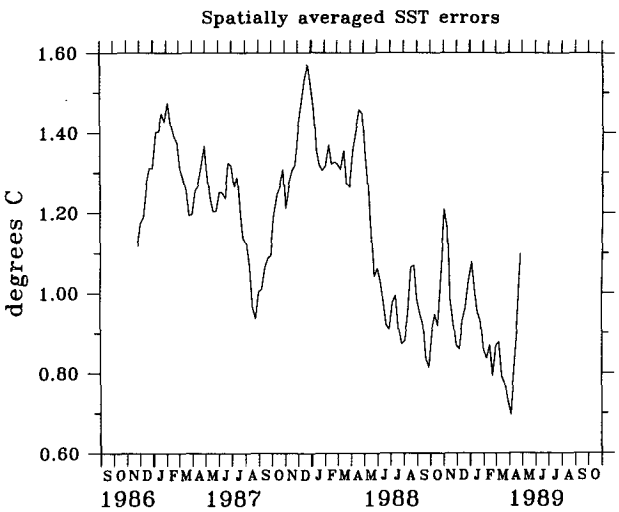

FIG. 4. Spatially averaged SST errors from the optimal estimates. The weekly averages of AVHRR data were optimally averaged with an averaging interval of two weeks to reduce random errors and those from cloud cover gaps. The error estimates varied by nearly a factor of 2, both in time and spatially.

There are systematic differences between SST and mixed layer temperature T_m, which we estimated using the Levitus (1982) climatology. Because the Levitus data are somewhat sparse, we obtained weekly maps of the temperature offset by fitting these differences to the first EOF of SST and then interpolating the amplitude to weekly intervals. Although the offset was as large as 3°C in the summer, it had a negligible affect on the heat budget because only the derivatives are used in estimating the heat budget (2) and the spatial structure of the offset was smooth due to the sparseness of the data.

Climatological mixed layer depths were needed both for constraints on the model mixed layer and for comparisons of the annual signal of the model estimates. We used the mixed layer depths computed from the Levitus monthly climatology based on a criterion of 0.5°, consistent with the temperature difference used in the model and Kalman filter. Monthly maps of mixed

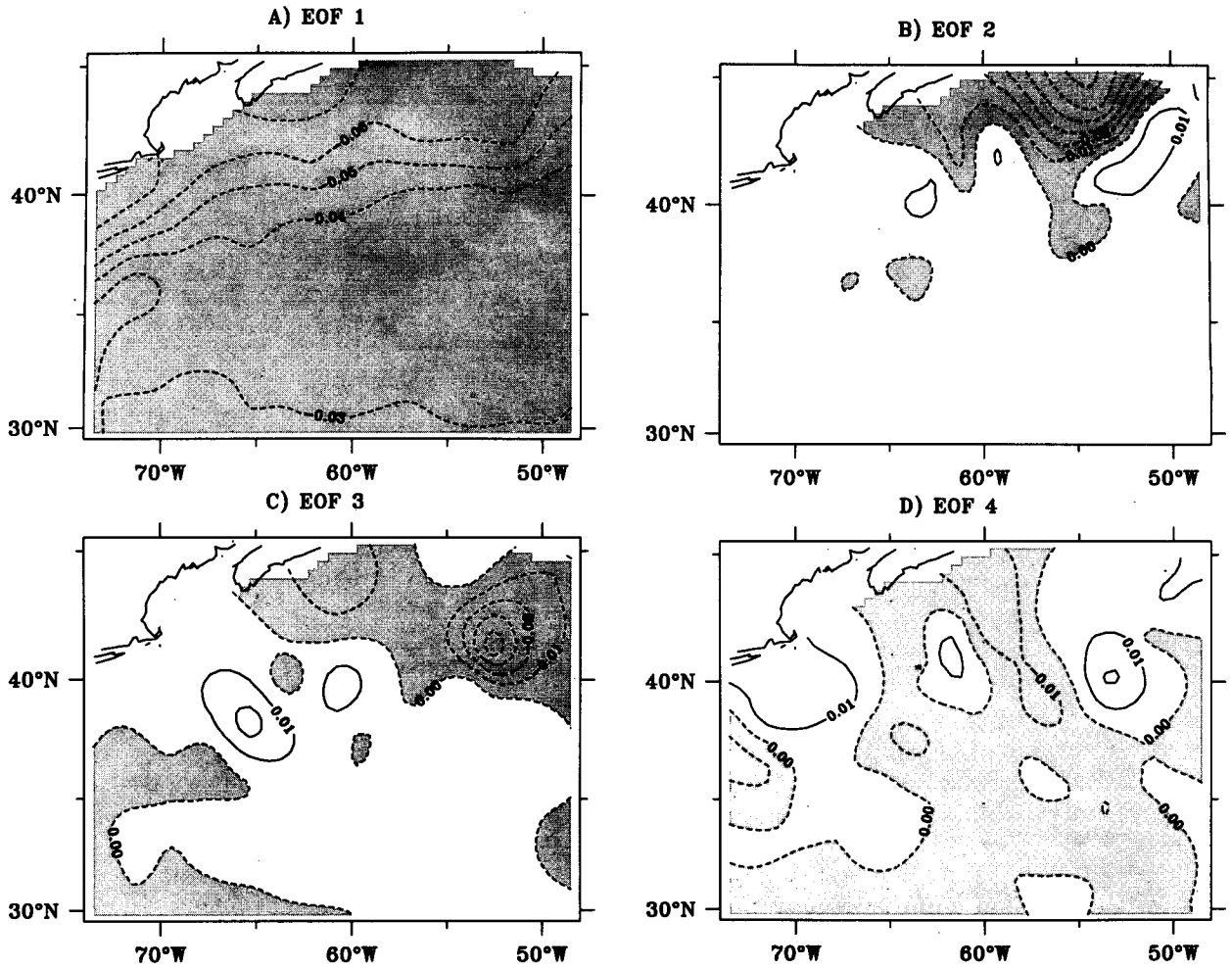

FIG. 5. Empirical orthogonal functions of temperature tendency. To reduce the computations and to smooth the surface flux estimates, the Kalman filter was formulated in terms of the amplitudes of EOFs of temperature and temperature tendency, computed from the SST data. The first four modes of temperature tendency are shown here, with negative regions stippled. Units are degrees Celsius per day.

layer depth at a spatial resolution of 1° × 1° were interpolated temporally and spatially to give twice-monthly values on the model grid.

To estimate vertical entrainment from the turbulent kinetic energy balance, we needed to compute the shortwave solar radiation $q(0)$. To determine the daily averaged $q(0)$ values, we estimated the clear-sky radiation values and inferred the (average) cloud cover from the 6-hour-accumulated $q(0)$ data from ECMWF, as described in QK. The ECMWF estimates of net surface heat flux Q_{net}, also modified to represent daily averages, were used to test the prognostic model and for comparison with the surface flux estimates.

5. Tests using synthetic data

To test the accuracy of the Kalman filter in estimating the net surface flux and to tune the error estimates, we first generated synthetic data using a known value of Q and then ran the Kalman filter on these data. Although good estimates are available for SST, the error in the temperature tendency in the data is not well defined, because $T(t + \delta t) - T(t)$ depends on the temporal correlation of the errors in the optimally averaged maps. Based on the e-folding scale of 5 days (see appendix A), SST values separated by a week should be virtually uncorrelated, but averages over two weeks, separated by a week, would have correlated errors. In addition, errors must be specified in terms of their modal distribution. For all of the analyses on synthetic data, we assumed that the temperature and temperature tendency model and data errors were distributed among the modes like temperature tendency itself, as given by the EOF decomposition.

To create the synthetic data, the mixed layer model was initialized with observed T_m and then run with a specified Q that remained constant for each week. The values of the mixed layer temperature T_m at the end of

each week and the weekly average of depth $\langle h_m \rangle$ were saved as "synthetic data." The surface flux used in the tests was derived from the ECMWF data, using the temporally averaged value plus two spatial modes obtained from an EOF analysis. The EOFs of both SST and temperature tendency were computed from the synthetic data for use in the Kalman filter. For each experiment, input amplitudes of the modes of Q/h_m were computed by projecting Q/h_m from the synthetic data onto the temperature tendency modes (EOFs). Although only two modes of Q were used, four significant modes of Q/h_m were obtained because of the variations in h_m. Input amplitudes of Q/h_m were compared with the amplitudes estimated using the Kalman filter.

The first test revealed the importance of an annual mean in reconstructing the surface flux estimate. In examining the initial estimates of the surface flux from the Kalman filter, we observed that no linear combination of the temperature tendency modes from the synthetic data could adequately reconstruct the mean surface flux estimated from the ECMWF data. To understand this, it is instructive to temporally average the heat equation (2) over a year. The first term on the left vanishes, except for interannual variations, and the average surface flux then balances the advection, diffusion, and entrainment terms,

$$\left\langle U \frac{\partial T_m}{\partial x} \right\rangle + \left\langle V \frac{\partial T_m}{\partial y} \right\rangle = \langle h_m A_T \nabla^2 T_m \rangle + \frac{\langle Q_{\text{net}} - q(-h_m) \rangle}{c_p \rho_0} - \Delta T \langle w_e \rangle, \quad (17)$$

where angle brackets denote the temporal average over a year. The dominant balance in (17) is between mean advection and surface heating therefore, the annual mean surface flux cannot be represented by a combination of the spatial modes of the time-varying temperature tendency. In subsequent tests, the surface flux was estimated as the sum of the ECMWF mean surface flux $\langle Q \rangle$ and a linear combination of temperature tendency modes, $\mathbf{F}$,

$$\frac{Q}{h_m} = \frac{\langle Q \rangle}{h_m} + \mathbf{F}(x)\alpha(t), \quad (18)$$

where the modal amplitudes α were contained in the state vector of the Kalman filter. There was no requirement that the modal amplitudes average to zero over a year, so that the actual mean surface flux differed somewhat in spatial structure from the ECMWF estimate.

The second synthetic test showed that it is necessary to retain smaller-scale structure in the mixed layer temperature. Using the EOFs of temperature $\mathbf{F}_T$ from the data, the temperature T_m at any time can be expressed as the temporal mean $\langle T_m \rangle$ plus the sum of modes

$$T_m(t) = \langle T_m \rangle + \mathbf{F}_T \beta(t) + T'_m, \quad (19)$$

where β is the vector of coefficients and T'_m is a residual not described by a subset of the EOFs. For each week the coefficients β of the modeled temperature were determined and were updated using the Kalman filter and the data for that week. When 10 modes were used for the synthetic tests and the residual was neglected, the Kalman filter essentially low-pass filtered the temperature data. At the next time step, advection by the Gulf Stream core reintroduced smaller-scale temperature structure, and this temperature change gave rise to erroneous small-scale structure in the temperature tendency $\partial T_m/\partial t$. Estimates that retained the temperature residual at each time step but updated the larger-scale temperature structure, β, gave more accurate results. In real data tests, the number of temperature modes was increased to 30 to retain smaller-scale structure. The number of modes used for the temperature update is not a critical parameter, because the only purpose in adjusting the temperature is to prevent a systematic drift away from the data.

The third synthetic test examined the accuracy of the retrieved amplitudes for four Q/h_m modes with varying values of the Kalman gain (Fig. 6). These tests suggested that the Kalman filter should be able to reliably extract at least two modes of Q/h_m from the actual data. The accuracy of the retrieval of the third and fourth modes is somewhat less than for the first and second modes; however, the contribution of the third (fourth) mode to the temperature tendency is only about 22% (20%) of the first mode. The modal amplitudes are comparable in Fig. 6 because the scaling factors were contained in the spatial modes themselves. The spatially averaged value of Q_{net} agreed well with the original value used to create the synthetic data; the largest discrepancy was a 10 W m^{-2} underestimate in the magnitude at about day 400. The averaged Kalman gain used for the values shown in Fig. 6 was about 0.5; larger gains produced even closer agreement. However, these tests did not include data noise, which would tend to degrade the comparisons. In the experiments with real data, four modes were again used, but the gain on each mode was determined separately, as described in the section 6.

6. Real data experiments

A series of tests were run using the SST data, which allowed us to make adjustments to the model and to the Kalman filter formulation as well as a correction to the mean SSH. Finally, we examined the sensitivity to the Kalman gain values. Thirty temperature modes were used in these experiments and up to four temperature tendency modes were used.

a. Model and Kalman filter adjustments

The first modification to the model was to introduce a constraint on mixed layer shoaling to make the model

more stable. The spatial and temporal resolution of the data did not allow us to resolve some of the mesoscale variations in the Gulf Stream or relatively rapid changes in temperature and heat flux; these smaller-scale variations, as well as actual errors in the data, constitute noise for this analysis. The presence of such noise in the temperature data induced rather large positive values of Q in localized regions, and the numerical model responded by abruptly decreasing the mixed layer depth. A return to a more typical surface flux in that region in the subsequent week then gave rapidly varying temperature T_m values because the mixed layer depth h_m was too small. This problem was remedied by allowing only a gradual decrease in depth: a maximum depth decrease of about 50% per week. This constraint did not appear to interfere with the rather rapid seasonal shoaling (about 20% per week) required in the spring in response to continuous positive surface flux forcing.

The second modification was a reduction in the horizontal diffusion of temperature. The relatively large horizontal temperature diffusion coefficient used by QK for the Kuroshio Extension model was reduced, by about a factor of 4, to about 2000 $m^2 s^{-1}$ to maintain the narrow warm core in the Gulf Stream, consistent with the SST data. However, it was not possible to reduce the horizontal diffusion coefficient for the mixed layer depth by that factor, because of the localized shoaling problem described above. Retaining a relatively large value of horizontal diffusion of the mixed layer depth (5000 $m^2 s^{-1}$) was determined to be the best method. Table 1 summarizes the model parameters used for the experiments described here, except as noted in the text.

The Kalman filter estimate (19) for the mixed layer temperature T_m had to be modified to slightly damp the residual T'_m. Because the temperature EOFs were derived from data only and did not reflect systematic biases of the model, the residual temperature variability became progressively noisier over a period of a few months, particularly near the boundaries. The Kalman temperature estimate used on the real data was given by

$$T_m(t) = \langle T_m \rangle + \mathbf{F}_T \beta(t) + \gamma T'_m, \qquad (20)$$

where γ was 0.8 for most experiments.

Tests on real data constraining the mixed layer depth to match the climatological mixed layer depth resulted in surface flux estimates Q_{net} consistently too large in the late spring (Fig. 7), compared with the spatially averaged surface flux estimates from the ECMWF and the Bunker values (Isemer and Hasse 1987). Even using a relatively weak constraint, $c = 0.3$ in (13), forced the mixed layer to be consistently deeper than that predicted by the model in the early spring because the monthly depth averages obtained from the Levitus data did not adequately resolve the rapid shoaling of the mixed layer in the spring, as was seen in a related analysis in the Kuroshio Extension (QK). Because the Kalman filter adjusts the ratio Q/h_m, a larger surface flux is required to achieve the same degree of warming when the mixed layer is too deep. Heat flux estimates without the mixed layer constraint compared favorably with the ECMWF estimates. In subsequent tests of the sensitivity to the Kalman gain for the other parameters, no mixed layer constraint was used.

b. Mean SSH correction

Some systematic differences were found between the temperature tendency predicted by the model and that from the SST data (Fig. 8a). As shown in Part II, the largest contribution to the tendency is advection and thus it was the most likely candidate for the systematic errors. A suggestion that there was an error in the mean Gulf Stream path was found in the comparison of the altimetric estimate with that from the Levitus data (Qiu 1994). The climatological mean Gulf Stream path is more than one degree of latitude south of the altimetric estimate at 73°W. Another area with a substantial discrepancy is in the vicinity of the New England Seamount Chain at 65°–62°W, where the climatological path is nearly 1° latitude north of the altimetric estimate. These discrepancies could be due to actual differences in the Gulf Stream path for the short time period over which the Geosat data were collected; however, the Gulf Stream does not meander much near 73°W, where the largest differences occur. If the velocity jet were misaligned there such that it was directed across the temperature front from the cold side to the warm side, it would produce a negative contribution to the temperature tendency in the model and thus would require a positive mean surface flux over the Gulf Stream core to match the observed SST. This is precisely what is suggested by the temperature tendency comparison (Fig. 8a).

Assuming that advection by the mean geostrophic currents was the dominant source of error, a correction to the mean SSH was made by minimizing the difference in temperature tendency for the model and the data; that is,

$$-\frac{\partial \psi}{\partial y}\left\langle \frac{\partial T}{\partial x} \right\rangle + \frac{\partial \psi}{\partial x}\left\langle \frac{\partial T}{\partial y} \right\rangle = -\left\langle \frac{\delta T_m}{\delta t} - \frac{\delta T_d}{\delta t} \right\rangle, \qquad (21)$$

where ψ is a streamfunction for mixed layer transport, T_m, T_d are the mixed layer temperatures from the model

TABLE 1. Model parameter values.

Parameter	Symbol	Value
Horizontal temperature diffusion	A_T	2000 $m^2 s^{-1}$
Horizontal depth diffusion	A_h	5000 $m^2 s^{-1}$
Temperature difference	ΔT	0.5°C
Time step	δt	2 h
Damping factor for T_m residual	γ	0.8

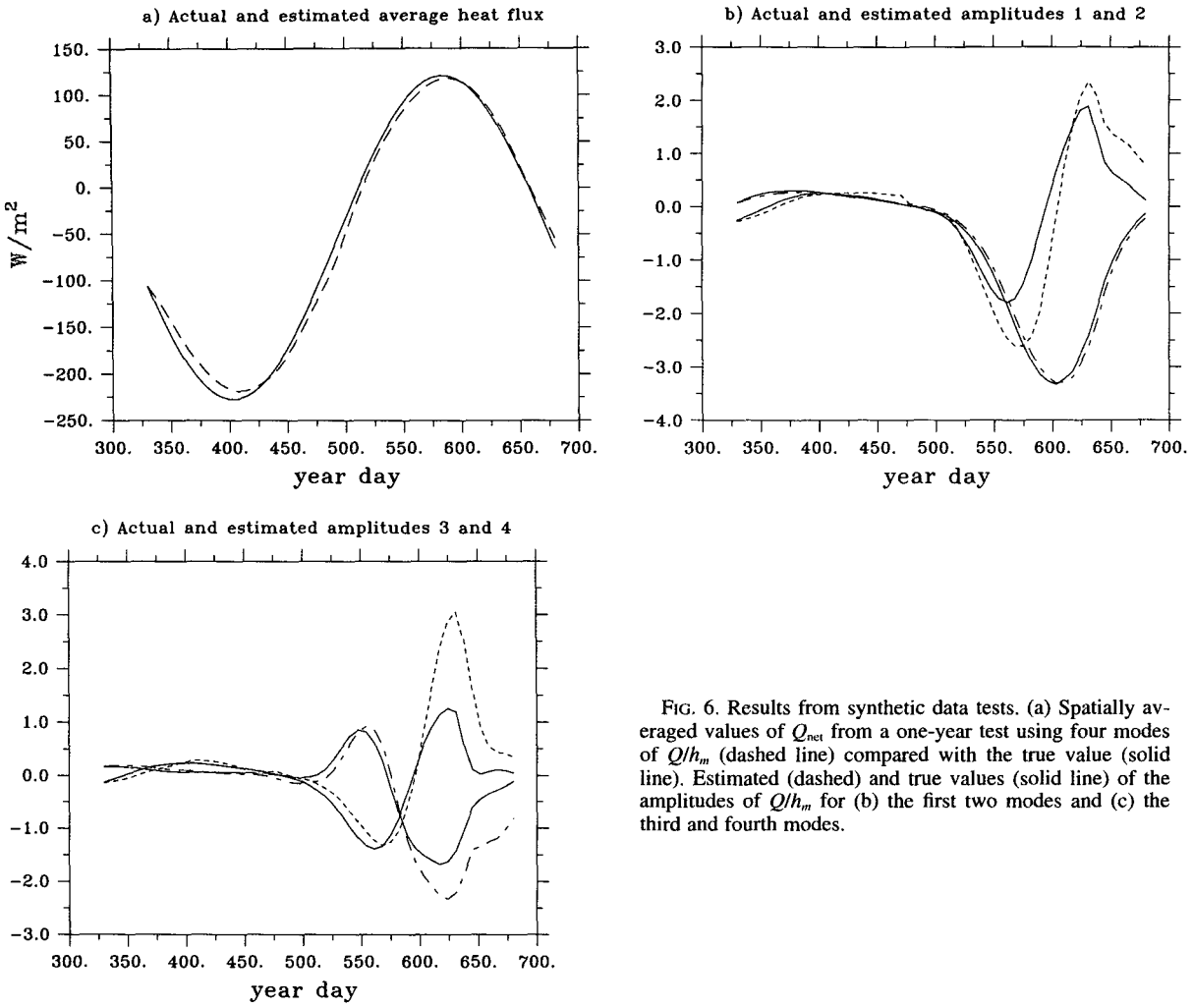

FIG. 6. Results from synthetic data tests. (a) Spatially averaged values of Q_{net} from a one-year test using four modes of Q/h_m (dashed line) compared with the true value (solid line). Estimated (dashed) and true values (solid line) of the amplitudes of Q/h_m for (b) the first two modes and (c) the third and fourth modes.

and data, respectively, and $\langle \cdot \rangle$ denotes the temporal average. The SSH correction is then given by $\delta\langle\eta\rangle = -f_0\psi/g$. The model/Kalman filter was run for 104 weeks to calculate the mean error in temperature tendency between data and model.

Finding a (correction to the) SSH field based on temperature advection is similar to inferring velocity from pairs of SST maps (Kelly 1989; Kelly and Strub 1992) and a similar procedure was used here. Grid points for which the estimated temperature errors in both maps exceeded 1.5°C were eliminated in computing the mean to prevent large erroneous SST values from dominating the SSH correction; the tendency error was set to zero for those points with negligible mean temperature gradients to keep the correction from becoming arbitrarily large. The best least squares fit to (21) was found, subject to a minimization of the magnitude of the solution ψ. The selected correction reduced the squared error in the mean temperature tendency by 33%; the root-mean-square size of the SSH correction was 0.037 m. The correction (Fig. 9) decreased the strength of the jet at73°W (Fig. 10) and made a northward jog in the path at the New England Seamount Chain (60°W). In addition, the northern recirculation gyre was elongated and the offshore flow near 44°N, 57°W was eliminated. The model/Kalman filter run with the corrected mean SSH had much smaller mean differences between temperature tendency in the model and in the data (Fig. 8b), but differences as large as 0.05°C/day persisted in some regions. Based on the analysis of the heat budget in Part II, advection by Ekman transport was generally larger than advection by geostrophic currents on the intermediate spatial scales (hundreds of km), and, therefore, it is a likely candidate for the residual errors in Fig. 8b. Gridded wind products currently available lack the spatial resolution to produce an accu-

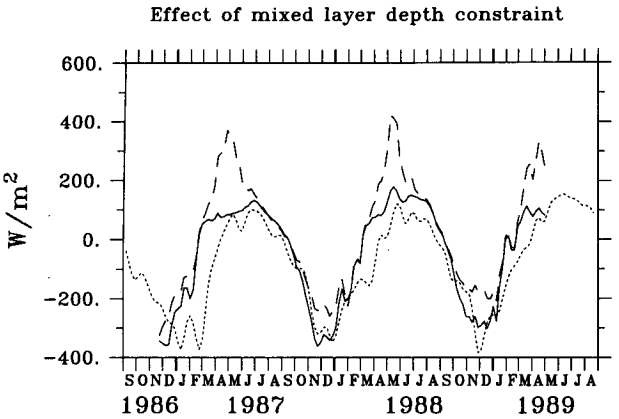

FIG. 7. The effect of a climatological mixed layer depth constraint. Spatially averaged surface flux Q_{net} from the ECMWF data (dotted line) and from the model without (solid line) and with (dashed line) a weak constraint to match climatological mixed layer depths. The the depth constraint prevented the rapid shoaling of the mixed layer model and caused unrealistically large heat fluxes in the spring.

rate estimate of the Ekman transport in the vicinity of these strong temperature gradients.

b. *Sensitivity to Kalman gain*

A series of tests was performed on real data to determine the optimal values of the gain for the temperature and Q/h_m. A relatively high gain was required for the 30 temperature modes. The gain was optimized by examining the difference between the data and the temperature T_m predicted by the model, which is known as the "innovation" (Dee et al. 1985). Ideally, this quantity, $\mathbf{d}(k) - \mathbf{q}(k|k-1)$ in (8), should have a white spectrum, indicating that all the useful information has been extracted by the Kalman filter, that is, that corrections at each time step are uncorrelated. Spectra for the first mode for gains that averaged approximately 0.6 and 0.8 are shown in Fig. 11. The spectral densities at the lowest frequencies are about an order of magnitude larger than those at higher frequencies for the low gain (Fig. 11a), compared with only a slight increase at low frequencies for the higher gain (Fig. 11b). The spatially averaged temperature T_m from the Kalman filter with the higher gain was considerably less noisy compared with the temperature data (not shown), although there was a consistent underestimate of the temperature in the late winter and early spring.

Experiments varying the gain for the modes of Q/h_m suggested a relatively high gain was needed for the first mode and that smaller gains were needed for higher modes. The temperature tendency modes, like the temperature modes, were scaled so that their expected amplitudes using the Kalman filter would be approximately the same size. Actually, this would only be true if the temperature tendency in the model had the same modal distribution of variance as the temperature tendency in the data. However, probably because the errors in advection were relatively large, higher modes in the model had disproportionately more energy than in the data. Therefore, gains for all the modes (here we used four temperature tendency modes to estimate the surface flux) were optimized to make the innovation spectra nearly white. This produced estimates of Q_{net} that compared favorably with the ECMWF estimates (Fig. 12). The spatial averages of Q_{net} shown here are most sensitive to the gain for the first mode; higher modes produce more spatial structure in the surface fluxes. Spatially averaged estimates of Q_{net} corresponding to a relatively low temporally averaged gain (0.4 for the first mode and 0.06 for higher modes) appreciably underestimated the wintertime (negative) surface fluxes (Fig. 12) and overestimated the spring

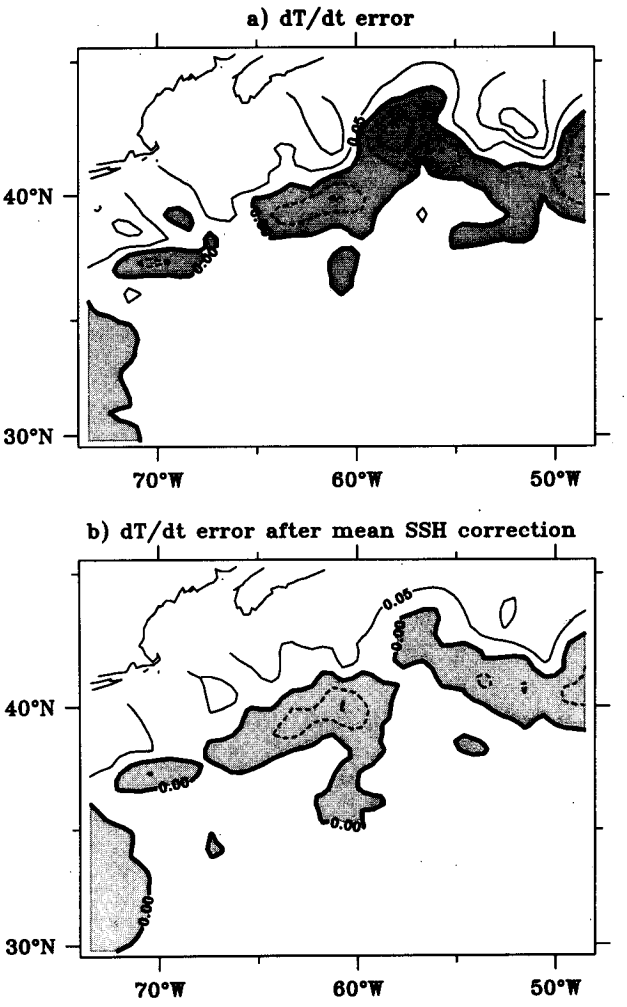

FIG. 8. The error in temperature tendency before and after a mean SSH correction. (a) The temporal average of the difference between the temperature tendency of the AVHRR data and of the Kalman tendency estimates had values as large as 0.1°C/day. (b) The variance of these errors was reduced substantially by a mean SSH correction.

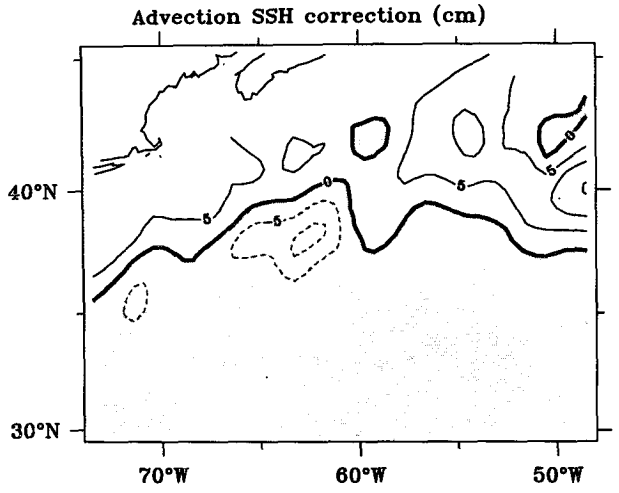

FIG. 9. The mean SSH correction applied to the altimeter data. Assuming the error in temperature tendency (Fig. 8a) was due to a mean advection error, the mean velocity correction (and SSH correction) which would minimize this error, was computed. This correction weakened the flow near 70°W and east of 57°W, and shifted the Gulf Stream farther north from 60° to 66°W.

(positive) surface flux, compared with the ECMWF estimates and the surface fluxes for a higher gain (0.8 for the first mode and 0.17 for higher modes).

In addition to determining the Kalman gain, the relative errors of the model and the measurements determine the amount of smoothing by the Kalman smoother. For example, for the higher gain the smoother does not substantially change the estimate (Fig. 13a); whereas for a relatively low gain (about 0.17), the smoother significantly alters the initial estimate (Fig. 13b). Summing over all four modes shows the effect of the smoother on the estimate of Q/h_m (Fig. 13c). Assuming errors in the modes are independent, the total error was computed as the root-mean-square of the errors for the four modes; these values are relatively small, typically 0.015°C/day, with the largest values in December 1987 when SST data were sparse. The larger errors at the end of the time series are the errors from the initial Kalman estimate, which is the same for the smoothed estimate because the smoother starts at the end of the time series, reducing the errors as it smooths.

Using the smoothed estimates shown in Fig. 13, the temporal average of the surface flux was computed for both the model estimate and for ECMWF (Fig. 14). Because the surface flux clearly had a trend toward more positive values and because of the calibration problem in the first half of 1987 described in the appendix, the two-year period over which the estimates were averaged was May 1987–April 1989. As discussed in section 5, the mean of the surface flux estimates using the Kalman filter (Fig. 14a) will not necessarily match the mean from the ECMWF data (Fig. 14b), although it was added to the modes to get the total estimate.

7. Discussion

The annual mean net surface heat flux from the model/Kalman filter differs somewhat from the mean of the ECMWF surface fluxes (Fig. 14), primarily in that there are regions along the mean Gulf Stream path where the negative core is quite weak. These regions generally correspond with the regions of large (negative) differences between the temperature tendency in the model and in the data (Fig. 8b). These errors may account for most of the differences in surface flux along the Gulf Stream core; for example, an error of −0.03°C/day, such as that at 40°N, 60°W in Fig. 8b, with an annual-average mixed layer depth of 100 m,

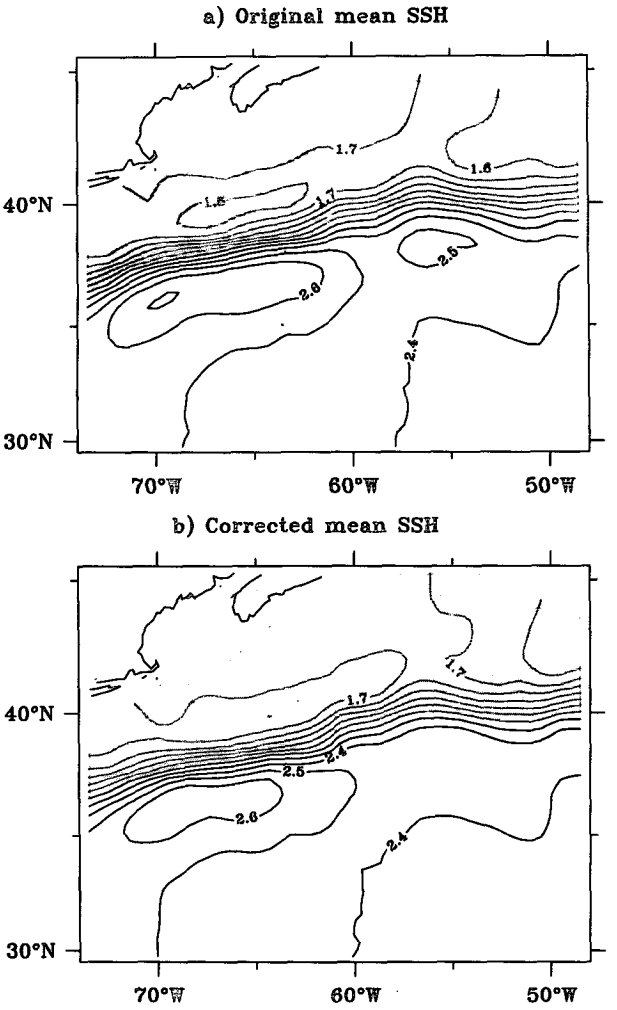

FIG. 10. The mean SSH before and after the correction. (a) The mean SSH computed by Qiu (1994) and (b) the mean SSH with the correction in Fig. 9 added. The northern recirculation gyre was elongated and the southern gyre was shortened by the correction.

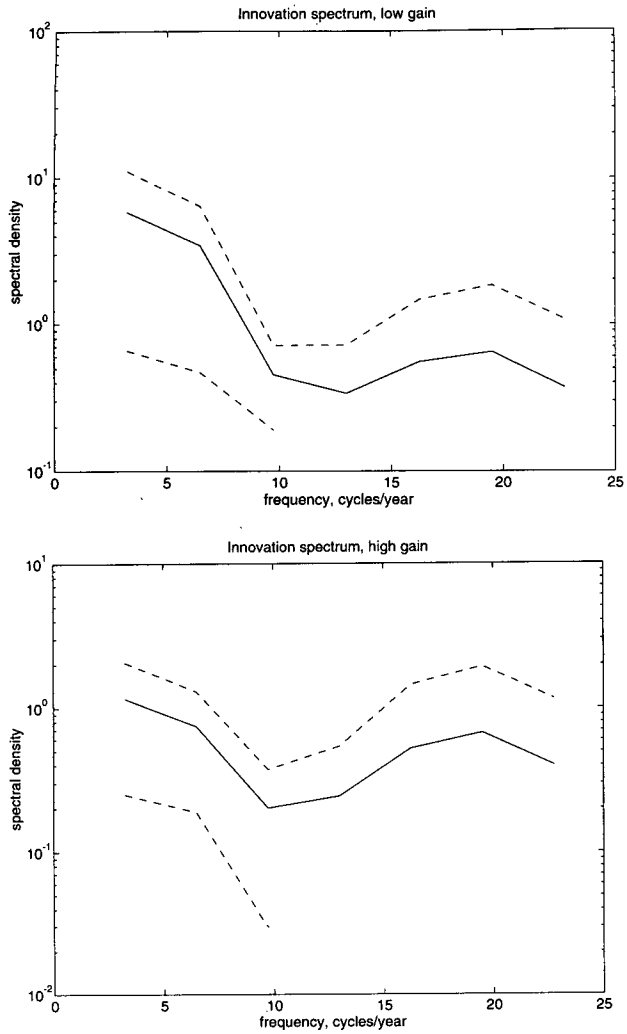

FIG. 11. Power spectra of the temperature innovation for low and high gains. The difference between the SST data and the Kalman temperature estimate, known as the innovation, was examined to optimize the Kalman gain. (a) The low gain produced a red spectrum, suggesting that insufficient information was being extracted from the data. (b) A higher gain produced a nearly white spectrum.

would give an error of about 140 W m^2. Subtracting this from the estimated value (Fig. 14a) of about -70 W m^2 gives an annual-average surface flux consistent with the -200 W m^2 value of the Bunker climatological value for the Gulf Stream core (Isemer and Hasse 1987). North of the Gulf Stream, the model/Kalman filter estimates are negative and the Bunker climatology suggests a region of positive mean surface flux; this is consistent with the positive errors in temperature tendency, which contribute a negative bias to the surface flux. In the far northeast corner of the model domain, the errors in temperature tendency are more complicated and, therefore, cannot explain discrepancies with the Bunker climatology; however, along the entire eastern boundary of the model domain, SST errors are relatively large. Some of the differences are undoubtedly due to the relatively coarse spatial resolution of the ECMWF estimates.

The spatially averaged time series of surface flux agreed surprisingly well with the ECMWF estimates (Fig. 12), surprisingly because the methods are almost entirely independent. Although the ECMWF atmospheric model uses SST maps derived from AVHRR data and our method uses AVHRR data as well as the ECMWF winds, the mixed layer model infers the net surface heat flux from changes in the oceanic mixed layer, rather than calculating them using bulk formulas. The similarity of the estimates suggests that the errors in either method, at least in a spatially averaged sense, are relatively small. The combination of the mixed layer model and the Kalman filter yielded more than two years of weekly maps of net surface heat flux estimates (Caruso et al. 1995).

The estimation procedure was quite efficient because of the use of modes in the Kalman filter, rather than adjusting the values at each model grid point. The entire time series can be calculated in less than 1.5 hours on a SUN SPARC 10 workstation. There are, however, some important drawbacks to solving the problem with modes. One problem is that the spatial structure of the temperature error is lost. Although the error varies substantially with time (Fig. 4), the error also varies by a factor of 2 spatially. In the modal formulation, the temperature error is spatially averaged and then distributed in a fixed way among the modes, so that the gain is reduced throughout the region during times of large average errors. If the temperature and the temperature tendency at each grid point were contained in the state

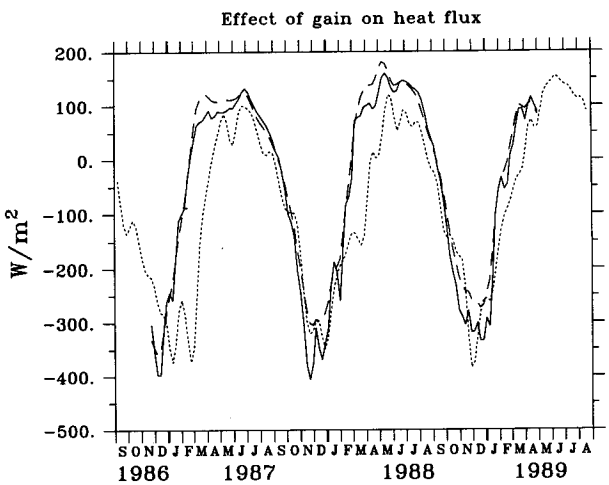

FIG. 12. Net surface heat flux for low and high Kalman gains. Spatially averaged surface flux Q_{net} for a relatively low gain (dashed line) and for a high gain (solid line), compared with the ECMWF estimates (dotted line). Negative surface fluxes (wintertime) are underestimated and positive surface fluxes (spring) are overestimated for the low gain, relative to the estimates for high gain and from the ECMWF.

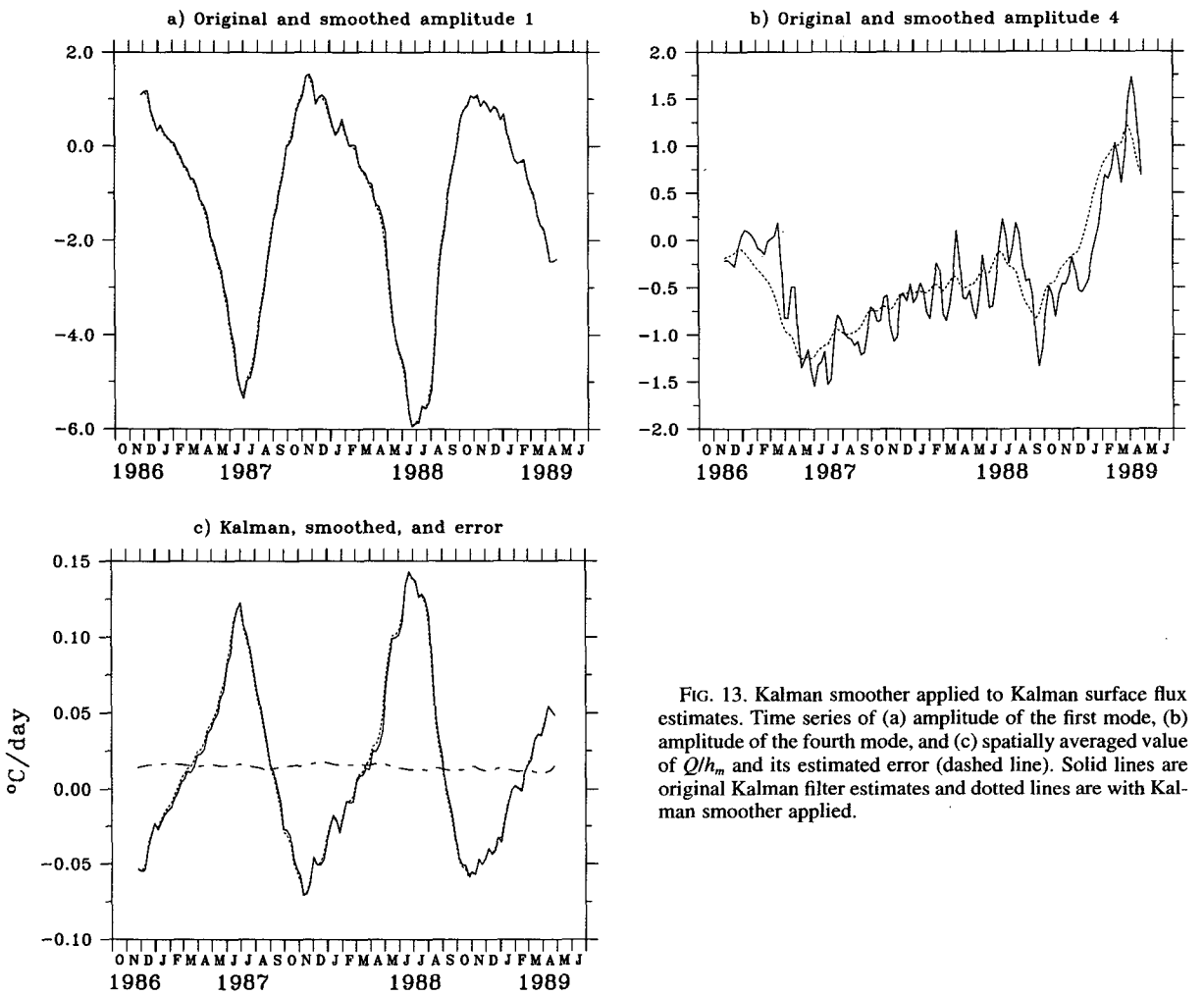

FIG. 13. Kalman smoother applied to Kalman surface flux estimates. Time series of (a) amplitude of the first mode, (b) amplitude of the fourth mode, and (c) spatially averaged value of Q/h_m and its estimated error (dashed line). Solid lines are original Kalman filter estimates and dotted lines are with Kalman smoother applied.

vectors, then the error could be computed for each point individually and the gain would vary both in time and in space. This would allow the gain to decrease dramatically in the northeastern part of the region, which remained cloud covered throughout much of the winter of 1987/88, and would have damped the oscillations in the surface flux estimates in December 1987 (Fig. 13c).

It was also not clear what the absolute error for the temperature tendency should be, even given a good estimate of the SST error ϵ. For an accurate estimate it would be necessary to know the temporal decorrelation of ϵ because the maps combine several weeks of data into each estimate. Assuming that the errors were relatively well correlated from one week to the next, only a fraction of the expected $\sqrt{2}\epsilon$ would be contained in the difference. It was also unclear how to distribute this error among the modes; therefore, in particular, the magnitude of the variations in spatial structure is not well constrained. Nevertheless, the relative contributions of the modes to the final estimate was robust with respect to any variation of the gain: a very small gain could not reduce the rms amplitudes of the higher modes relative to that of the first mode, nor could a large gain increase the amplitudes of the higher modes.

Another problem with the simple Kalman filter implementation was that there was no feedback between the errors in temperature and the errors in the surface flux estimates. Each Kalman filter was treated independently, although the measurement errors for each were scaled with the errors in the SST maps, so that the gains also covaried.

Finally, there are limitations with the data and the model. Both the mesoscale variations in the Gulf Stream and the temporal variations of surface fluxes cannot be resolved with the available altimetric data and these unresolved fluctuations create a relatively large source of error, from which the smoothed heat flux estimates must be extracted by the Kalman filter. In addition, AVHRR data are notoriously sparse in the wintertime, when surface flux reaches its extreme negative value. Currently available wind fields do not have

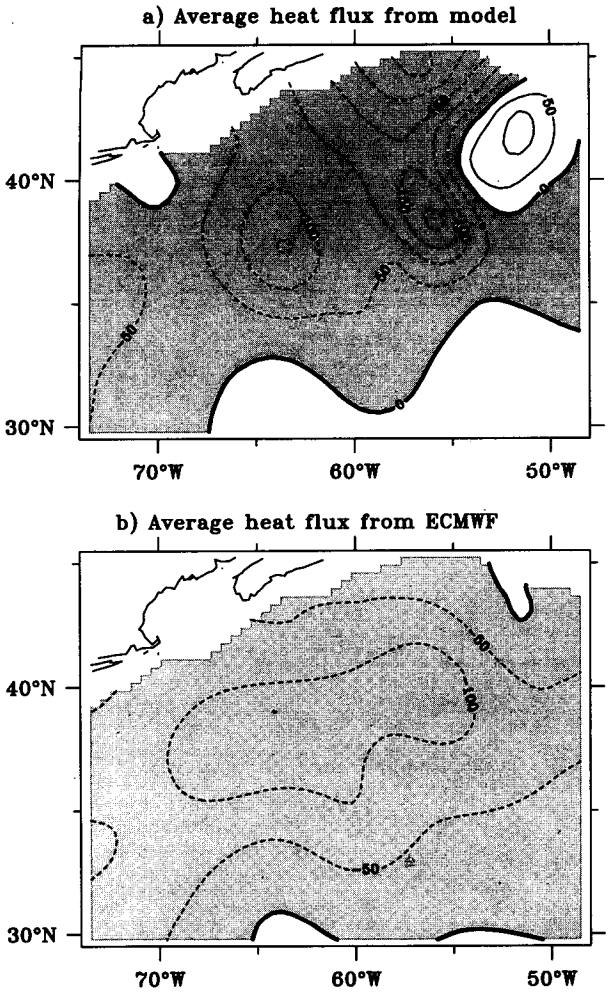

FIG. 14. Annual mean surface flux for Kalman estimate and for ECMWF. Two-year average of surface flux estimate from (a) the model/Kalman filter and (b) from ECMWF. Note the relatively complicated spatial structure of the negative region along the core of the Gulf Stream and the regions of positive surface flux.

as high a spatial resolution as the altimetric velocity fields and this may adversely affect the computation of advection due to Ekman transport, or temperature changes due to vertical entrainment. The contribution of entrainment was relatively small; however, this was not the case for advection from Ekman transport, as discussed in Part II. In the future, high-resolution wind fields from satellite scatterometers will allow more accurate wind fields and this improvement would warrant analysis with a more accurate mixed layer model. Finally, the analysis of the errors in the temperature tendency suggested some systematic advection errors, which are probably due in part to the mean SSH. A partial correction for this problem was obtained, but rather small errors (the correction computed here had a rms amplitude of only 0.037 m) cause large errors in advection in a region of such strong currents and strong temperature gradients. A better estimate of the mean SSH, which could be obtained with a better gravitational geoid, would be helpful here.

A detailed analysis of the mixed layer heat budget appears in the second half of this analysis, Part II: The Upper Ocean Heat Balance.

8. Summary and conclusions

Using data from a satellite-mounted radar altimeter and an infrared radiometer, along with winds from an atmospheric model, we have estimated the net surface heat flux required to balance the mixed layer heat budget. Our method combined a simple numerical mixed layer model with a Kalman filter to assimilate both temperature and temperature tendency. The upper ocean heat budget included eddy diffusion and advection calculated in the model using velocities primarily derived from the sea surface height field measured by the altimeter.

To reduce the computational and storage requirements, the Kalman adjustment was made using a finite number of modes of temperature and temperature tendency. The use of modes made the Kalman filter very efficient. A series of experiments performed on synthetic temperature data suggested some modifications to the Kalman formulation and suggested that it was possible to retrieve the amplitudes of several modes of the term $Q_{\text{net}}/(c_p \rho h_m)$, where h_m is the mixed layer depth determined by the mixed layer model.

Experiments performed on the actual data suggested that better surface flux estimates could be obtained by allowing the model to predict the mixed layer depth rather than by adjusting the depth toward a climatological value. Systematic errors in the temperature tendency appeared to be due to errors in advection. A correction for errors in the mean SSH from the altimeter was applied, assuming the errors were due to the advection by mean geostrophic currents. The residual errors after this correction may have been due to errors in advection by Ekman transport, due to errors in the wind field.

Because the model errors and the measurement errors for temperature tendency are poorly known, no objective method for setting the Kalman gain was available. Optimal gains for temperature and temperature tendency were determined by requiring the frequency spectrum of the model/data errors to be "white."

The agreement between the time series of spatially averaged surface flux and that obtained from the ECMWF atmospheric model was surprisingly good, with the largest discrepancies occurring in February and March, associated with mixed layer shoaling. The temporally averaged surface flux estimates from the mixed layer model and that from ECMWF were substantially different; these differences were due in part to errors in the estimate of advection.

APPENDIX A

Computation of the SST maps

Weekly averaged AVHRR data are available for the North Atlantic in either daytime or nighttime versions; however, much of the nighttime data was flagged as cloud contaminated, and thus we chose to use only the more complete daytime dataset. There were some calibration errors in the AVHRR data for the first half of 1987 (Bates 1994), which were reflected in comparisons of the monthly mean SSTs from the MCSST version of the AVHRR data with the monthly means from the COADS data, as a function of latitude. An additional analysis by Bates suggested that the correction could alternatively be parameterized as a function of SST (J. Bates 1993, personal communication). Therefore, a correction for the weekly average SST was computed by interpolating tables of the AVHRR bias as a function of SST and month.

The AVHRR daytime data were averaged over a period of two weeks using an optimal average (Chelton and Schlax 1991), which is a straightforward extension of the usual objective map. The optimal average requires a temporal covariance function for SST, which we estimated using a test series of 1-km resolution AVHRR images for September–October 1988, which had been flagged for clouds. The covariance function used was exponential in time:

$$C(t) = V_s \exp(-|t|/T_s) + V_n \exp(-|t|/T_n), \quad \text{(A1)}$$

where V_s, V_n are the SST signal and noise variances, respectively, and T_s, T_n are their characteristic times. The main problem with using AVHRR data to estimate the covariance function is that noise in the AVHRR data may shorten the apparent decorrelation times for the signal; however, in this case the decorrelation times appeared to be quite distinct. The covariance estimates from the decimated data showed an abrupt drop at 12 h, suggesting that the primary AVHRR error is uncorrelated between images. Using a value for V_n of $1°C^2$ and a value for T_n of 1 h, the best fit of (A1) to the estimated SST covariances gave a value for T_s of about 5 days. The SST variance V_s had a spatially averaged value of about $3.4°C^2$, relative to the temporal mean over two months.

To make the estimated errors of the maps using the weekly average data consistent with the covariance function, we removed an annual mean from the data before the optimal estimate and then added it back to the data afterward. The annual mean was computed by a least squares fit of once- and twice-per-year harmonics to the SST data at each point.

The use of the weekly average SST values, rather than AVHRR image data, to generate a two-week average, required some adaptations of the optimal estimation algorithm. The only information retained in the one-week averages is the number of data N used in each estimate, not the times and dates of the original data. Based on Monte Carlo simulations of 50 different random distributions of image times within a week, we found that the estimated error for the one-week average was primarily a function of the number of images used. The two-week average was even less sensitive to the distribution of the times of the data within each individual week. Therefore, one could estimate the error associated with each weekly average using only the number of data N used in that week and then average the values and errors from two weekly averages. However, it was actually more accurate to create "fake" data and use the optimal average algorithm. For each weekly average we repeated the value N times and assigned random dates during the week to the values, as if there were N separate measurements. We then used this much larger set of data to make the optimal maps. The other modification was to limit the amount of data used for each two-week average: a total of five weeks of data was used to make each optimal estimate. If no data were available during the five weeks at a given grid point, no estimate was made. A two-week optimal estimate was generated each week, so that the maps represent a running average of the SST data.

Acknowledgments. The authors thank J. Price and T. Joyce for helpful discussions regarding this analysis and R. Miller for suggestions on the implementation of the Kalman filter. S. Lentz carefully read the manuscript and suggested important clarifications. S. Singh patiently computed several versions of the optimal SST maps, and M. Caruso provided programming support for the data processing. We appreciate the generous contributions of V. Halliwell in supplying cloud-flagged AVHRR images for the optimal map tests and of J. Bates for supplying an empirical correction for the AVHRR weekly averaged data. Geosat altimeter data were obtained on CD-ROM from the NOAA National Oceanographic Data Center. AVHRR data were provided by the NASA Physical Oceanography Distributed Active Archive Center (PODAAC) at the Jet Propulsion Laboratory/California Institute of Technology. The ECMWF wind fields and surface heat flux estimates were obtained from the National Center for Atmospheric Research. This research was supported by NOAA through the Atlantic Climate Change Program under Contract NA16RC0468-01 and by the Office of Naval Research under Contract N00014-92-J-1656 (Kuroshio Extension Regional Experiment).

REFERENCES

Bates, J., 1994: A decade of multispectral sea surface temperature observations from space. *Adv. Space Res.*, **14**(3), 5–(3)14.

Caruso, M. J., S. Singh, B. Qiu, and K. A. Kelly, 1995: Monthly Atmospheric and Oceanographic Surface Fields for the western North Atlantic during the Geosat ERM, WHOI Tech. Rep., WHOI-95-05.

Chelton, D. B., and M. G. Schlax, 1991: Estimation of time-averaged chlorophyll concentration from irregularly spaced satellite observations. *J. Geophys. Res.*, **96**, 14 669–14 692.

Cheney, R. E., W. J. Emery, B. J. Haines, and F. Wentz, 1991: Recent improvements in Geosat altimeter data. *Eos Trans. Amer. Geophys. Union,* **72,** 577.

Dee, D. P., S. E. Cohn, A. Dalcher, and M. Ghil, 1985: An efficient algorithm for estimating noise covariances in distributed systems. *IEEE Trans. Automat. Control,* **AC-30,** 1057–1065.

Fukumori, I., J. Benveniste, C. Wunsch, and D. B. Haidvogel, 1993: Assimilation of sea surface topography into an ocean circulation model using a steady-state smoother. *J. Phys. Oceanogr.,* **23,** 1831–1855.

Gaspar, P., and C. Wunsch, 1989: Estimates from altimeter data of barotropic Rossby waves in the northwestern Atlantic Ocean. *J. Phys. Oceanogr.,* **19,** 1821–1844.

Isemer, H.-J., and L. Hasse, 1987: *The Bunker Climate Atlas of the North Atlantic Ocean.* Vol. 2: *Air–Sea Interactions.* Springer-Verlag, 252 pp.

Kalman, R. E., 1960: A new approach to linear filtering and prediction problems. *J. Basic Eng. Trans. ASME,* **82D,** 35–45.

Kelly, K. A., 1988: Comment on "Empirical orthogonal function analysis of advanced very high resolution radiometer surface temperature patterns in Santa Barbara Channel" by G. S. E. Lagerloef and R. L. Bernstein, *J. Geophys. Res.,* **93,** 15 753–15 754.

——, 1989: An inverse model for near-surface velocity from infrared images. *J. Phys. Oceanogr.,* **19,** 1845–1864.

——, and S. T. Gille, 1990: Gulf Stream surface transport and statistics at 69 W from the GEOSAT altimeter. *J. Geophys. Res.,* **95,** 3149–3161.

——, and P. T. Strub, 1992: Comparison of velocity estimates from AVHRR in the coastal transition zone. *J. Geophys. Res.,* **97,** 9653–9668.

——, and D. R. Watts, 1994: Monitoring Gulf Stream transport by radar altimeter and inverted echo sounders. *J. Phys. Oceanogr.,* **24,** 1080–1084.

Levitus, S., 1982: *Climatological Atlas of the World Ocean.* NOAA Prof. Paper No. 13, U.S. Govt. Printing Office, 173 pp.

Liu, W. T., and C. Gautier, 1990: Thermal forcing on the Tropical Pacific from satellite data. *J. Geophys. Res.,* **95,** 13 209–13 217.

Paduan, J. D., R. A. deSzoeke, and J. G. Richman, 1988: Balances of heat and momentum at 33.5°N, 127°W in the upper ocean during the mixed-layer dynamics experiment. *J. Geophys. Res.–Oceans,* **93,** 8147–8160.

Qiu, B., 1992: Recirculation and seasonal change of the Kuroshio from altimetry observations. *J. Geophys. Res.,* **97,** 17 801–17 811.

——, 1994: Determining the mean Gulf Stream and its recirculations through combining hydrographic and altimetric data. *J. Geophys. Res.,* **99,** 951–962.

——, and K. A. Kelly, 1993: Upper-ocean heat balance in the Kuroshio Extension region. *J. Phys. Oceanogr.,* **23,** 2027–2041.

——, ——, and T. M. Joyce, 1991: Mean circulation and variability of the Kuroshio Extension from Geosat altimetry data. *J. Geophys. Res.,* **96,** 18 491–18 507.

Stevenson, J. W., and P. P. Niiler, 1983: Upper ocean heat budget during the Hawaii-to-Tahiti shuttle experiment. *J. Phys. Oceanogr.,* **17,** 1984–1907.

Trenberth, K. E., W. G. Large, and J. G. Olson, 1990: The mean annual cycle in global wind stress. *J. Phys. Oceanogr.,* **20,** 1742–1760.

Yan, X.-H., J. R. Schubel, and D. W. Pritchard, 1990: Oceanic upper mixed layer depth determination by the use of satellite data. *Remote Sens. Environ.,* **32,** 55–74.